NANO LETTERS

pubs.acs.org/NanoLett

Letter

Efficient Production of Graphene through a Partially Frozen Suspension Exfoliation Process: An Insight into the Enhanced Interaction Based on Solid−Solid Interfaces

Kaixiang Pang,[#] Xiaoke Fang,[#] Chuanren Ye, Yuanhui Wang, Linlin Zhao, Chunhong Gong, Shuaishuai Zhou, Gai Zhao, Yanwu Zhu,[*] and Jingwei Zhang[*]

Cite This: *Nano Lett.* 2024, 24, 14102−14108

Read Online

ACCESS | Metrics & More | Article Recommendations | Supporting Information

ABSTRACT: Liquid phase exfoliation (LPE) offers a promising path for scalable graphene production, but struggles with high energy consumption and low yield, with over 99.99% of the input energy wasted. Here, we present an energy-efficient approach for producing graphene via partially frozen-suspension exfoliation (PFE). As opposed to traditional liquid−solid interfaces, the solid−solid interface enhances shear strength between the frozen solvent and graphite from about 40 N m^{-2} to 10^5 N m^{-2}. Additionally, the suspension flow transitions from turbulent to laminar, aligning graphite parallel to the flow direction and conducive to the effective utilization of shear force. Compared to conventional liquid-phase exfoliation (LPE), PFE improves energy efficiency by 10^2∼10^3 times. Furthermore, a production rate of 5 g h^{-1} has been achieved in a 10 L tank at an ultralow shear rate of 3 × 10^2 s^{-1}.

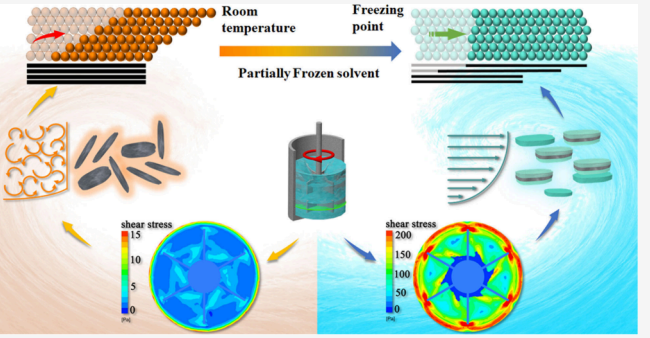

KEYWORDS: *partially frozen exfoliation, graphene, solid−solid interface, enhanced shear interaction*

Downloaded via UNIV SCIENCE AND TECHNOLOGY CHINA on March 5, 2026 at 01:17:07 (UTC).
See https://pubs.acs.org/sharingguidelines for options on how to legitimately share published articles.

With exceptional physical and chemical properties,[1−4] graphene[5] has identified itself in a wide range of applications such as thermal management,[6−10] energy storage,[11−13] and electric sensors.[14,15] Among various methods developed for scalable production of graphene,[16] liquid phase exfoliation (LPE) of graphite has been emerging as a promising approach for the scalable production of graphene suspension by utilizing the shear force to exfoliate graphite into single or few-layer graphene platelets in liquid media.[17−21] Avoiding harsh chemical processing involving strong oxidizing agents, together with the accessibility for industrial workflows, LPE offers a route to low-defect graphene, which is crucial for applications especially requiring high electrical conductivity such as for electromagnetic shielding.[22−28]

The early utilization of LPE often involves the high-frequency oscillation and cavitation effect generated by ultrasound, which, however, needs a high energy consumption of 10^{8-9} J g^{-1}[29,30] and is restricted by the local distribution of energy around the ultrasound rod. Coleman's group lowered the energy consumption to 10^7 J g^{-1} using a rotor-stator shear machine, which can generate a shear rate of higher than 10^4 s^{-1} in *N*-methyl-2-pyrrolidone (NMP) and produce graphene with a rate of 5.3 g h^{-1} in a 300 L tank.[19] By controlling the fluid dynamics in a laminar flow using a microslit at high pressure, Arao and co-workers further reduced the turbulent energy dissipation and achieved an energy utilization efficiency of 10^6 J g^{-1} in a homogenizer working with a shear rate of up to 10^7 s^{-1}.[18] Considering the van der Waals interlayer binding energy of 0.21−0.42 J m^{-2} (∼278−556 J g^{-1}, based on the specific surface area of 2630 m^2 g^{-1} for graphene)[31−33] in graphite, the energy consumption mentioned above means that only less than 0.01% of the input energy has been effectively utilized for the exfoliation of graphite in conventional LPE.

The large amount of input energy waste in LPE, mostly dissipated in the collision, squeezing, and flipping of the suspension components,[34] is closely related to the low viscosity solvents used as exfoliating medium in LPE, which often demonstrate a turbulent flow under the high shear rate. To improve the energy transfer from solvent to graphite, the effective shear transfer from solvent to graphite is specifically important, as the molecules in the liquid phase absorbed at the interface tend to slip under shear force.[35,36] To enhance the interaction between graphite and solvent, auxiliary reagents like polysaccharides have been used by utilizing the affinity

Received: September 4, 2024
Revised: October 17, 2024
Accepted: October 22, 2024
Published: October 25, 2024

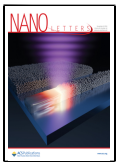

ACS Publications

© 2024 American Chemical Society

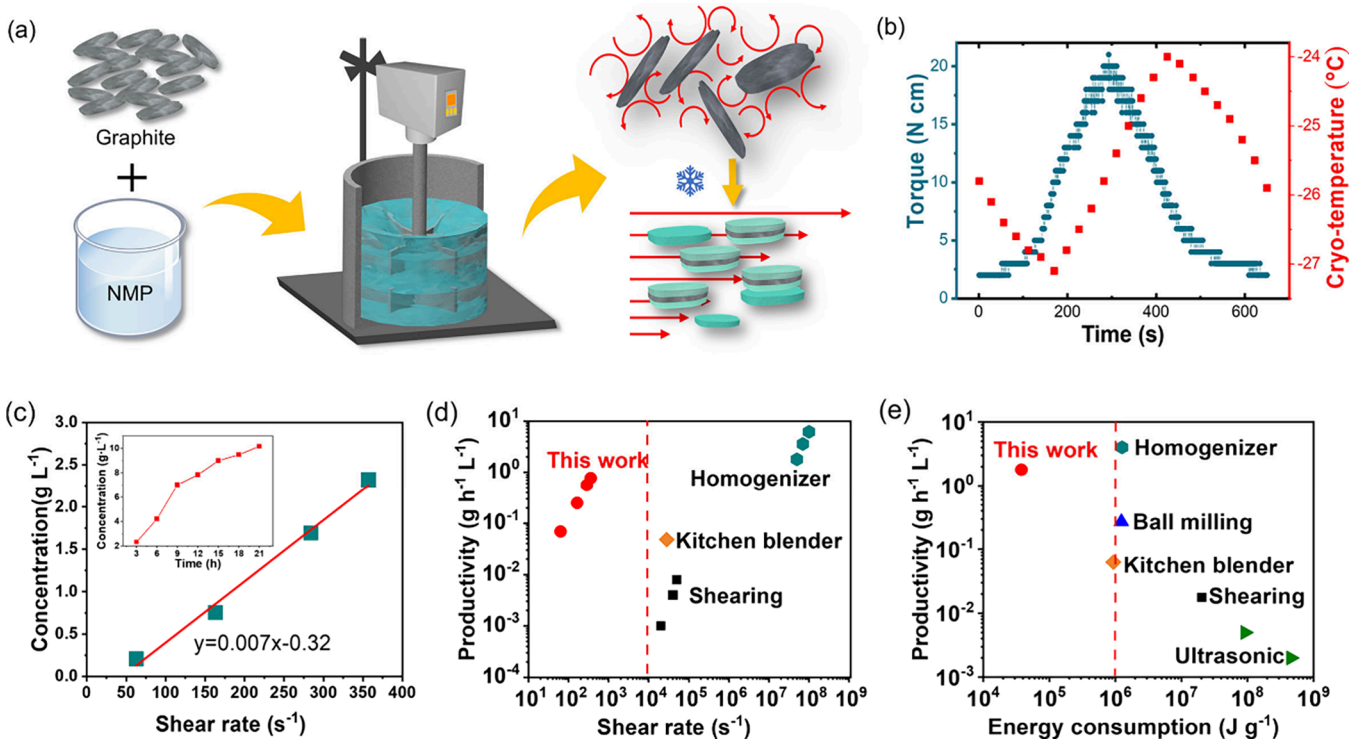

Figure 1. (a) Schematic of PFE with flow state change from liquid-based suspension (right-top) to PFS (right-bottom). (b) Changes of torque and coolant temperature in a freeze−thaw cycle. (c) Concentration of graphene suspension depending on shear rate and (inset) exfoliation time. (d) Shear rate and (e) energy consumption of exfoliation in this work compared to those of methods reported in the literature.[18,19,30,38,39]

between the nonpolar chains of polysaccharides and graphene; in this way the preparation efficiency of graphene was improved but repeating washes were needed to remove polysaccharides.[37] Without using any auxiliary reagent, we have achieved an increase of 50% in the exfoliation efficiency of graphite in *N*-octyl-pyrrolidinone (NOP) by decreasing the temperature from the room temperature (25 °C) to 0 °C, based on the enhanced NOP−graphite interface interaction in the higher viscosity NOP at 0 °C.[36] However, the exfoliation in NOP reaches a concentration of only 0.2 g L^{-1}, and the high cost of NOP would also restrict the scalability of exfoliation in NOP. Therefore, an efficient, yet low-cost, strategy to strengthen the solvent−graphite interface is still desired.

Inspired by the fact that a solid−solid interface generally has an enhanced interaction compared with a liquid−solid interface, herein we propose a partially frozen exfoliation (PFE) strategy in which the exfoliating liquid is frozen to form a solid−liquid interface. The PFE yields a largely enhanced shear strength of 10^5 N m^{-2} at the frozen NMP/graphite interface, compared to 40 N m^{-2} in liquid NMP. The viscosity of the suspension also increases greatly with the partially frozen NMP, decreasing the degree of turbulence in the stripping process. Consequently, the energy consumption for graphene exfoliation is reduced to 3.49×10^4 J g^{-1}, 10^2∼10^3 times lower than those needed in LPE. With this approach, an exfoliation efficiency of ∼5 g h^{-1} is achieved at an ultralow shear rate of 3×10^2 s^{-1} in a 10 L tank. The obtained graphene film exhibits an outstanding electromagnetic interference (EMI) shielding effectiveness of −27 dB at a thickness of 4 μm.

Figure 1a schematically illustrates the equipment used for PFE and the change in the suspension status upon freezing. The equipment consists of a jacketed stirred tank, a stirrer with real-time torque monitoring, and a refrigeration circulating pump to control the temperature of suspension in the tank via the jacket. The temperature was controlled by a cooling pump running periodically, which can modify the temperature setting by monitoring the torque change. At a speed of 400 rpm, the suspension is typically in a turbulent state at room temperature, as shown in Movie S1. As the jacket temperature gradually decreases below the freezing point (−24 °C) of NMP, the torque shows a remarkable increase, indicating an increase in the viscosity of the suspension, as shown in Figure 1b. Below the freezing point, the suspension is composed of graphite flakes, frozen NMP solid crystals, and not-yet frozen liquid NMP, named the partial frozen suspension (PFS), as shown in Movie S2. After cooling to −24 °C for 5 min, the PFS transits from a turbulent flow to a laminar one, as indicated by the decrease in Reynolds number from 5.7×10^3 to 34.7 (Supplementary Section 1).

The concentration of supernatant after centrifugation of processed PFS at 2000 rpm has been used to evaluate the efficiency of exfoliated graphite and for detailed characterizations below. Figure 1c shows that the concentration of the resulting supernatant product after 3 h of exfoliation linearly depends on the shear rate in the range of focus. The average shear rate was calculated by v/d (v, the blade linear velocity; d, the distance between the blade and the tank wall). By extrapolating the curve in Figure 1c to 0 g L^{-1}, a critical shear rate needed for the graphite exfoliation is estimated as 45 ± 5 s^{-1}, notably lower than 10^4 s^{-1} as previously reported in LFE.[18] The inset of Figure 1c shows the concentration of products monocratically increases with the stirring time, reaching 7 g L^{-1} after 9 h or 10 g L^{-1} after 21 h for a shear rate of 350 s^{-1} (stirring speed = 400 rpm), corresponding to a yield of 0.78 and 0.47 g h^{-1}, respectively. From the comparison shown in Figure 1d, the shear rates used in PFE are all lower than those

https://doi.org/10.1021/acs.nanolett.4c04329
Nano Lett. 2024, 24, 14102−14108

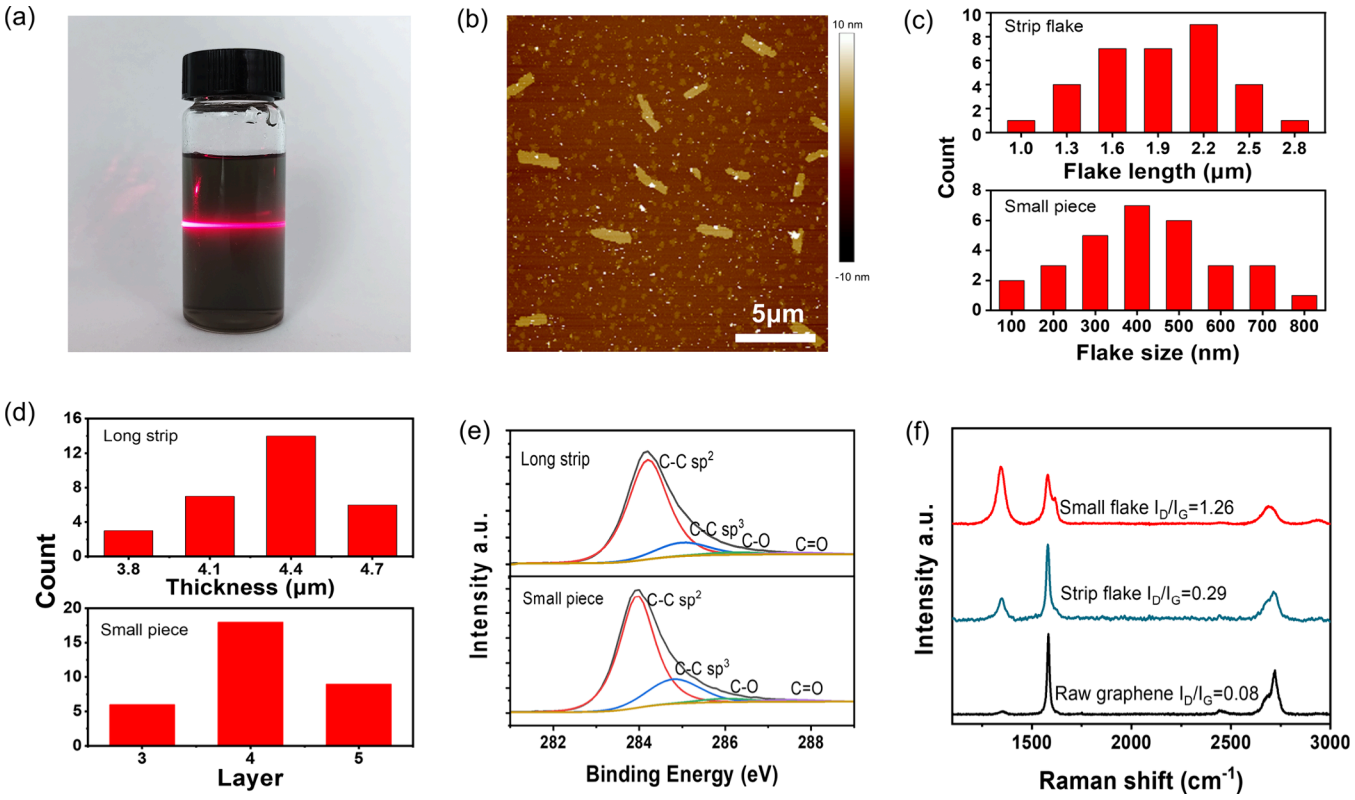

Figure 2. (a) Graphene dispersion showing the Tyndall effect. (b) AFM image of exfoliated graphite. (c) Flake size and (d) thickness distribution of two typical flakes. (e) XPS C 1s spectra for two flakes. (f) Typical Raman spectra of raw graphite and two graphene flakes obtained.

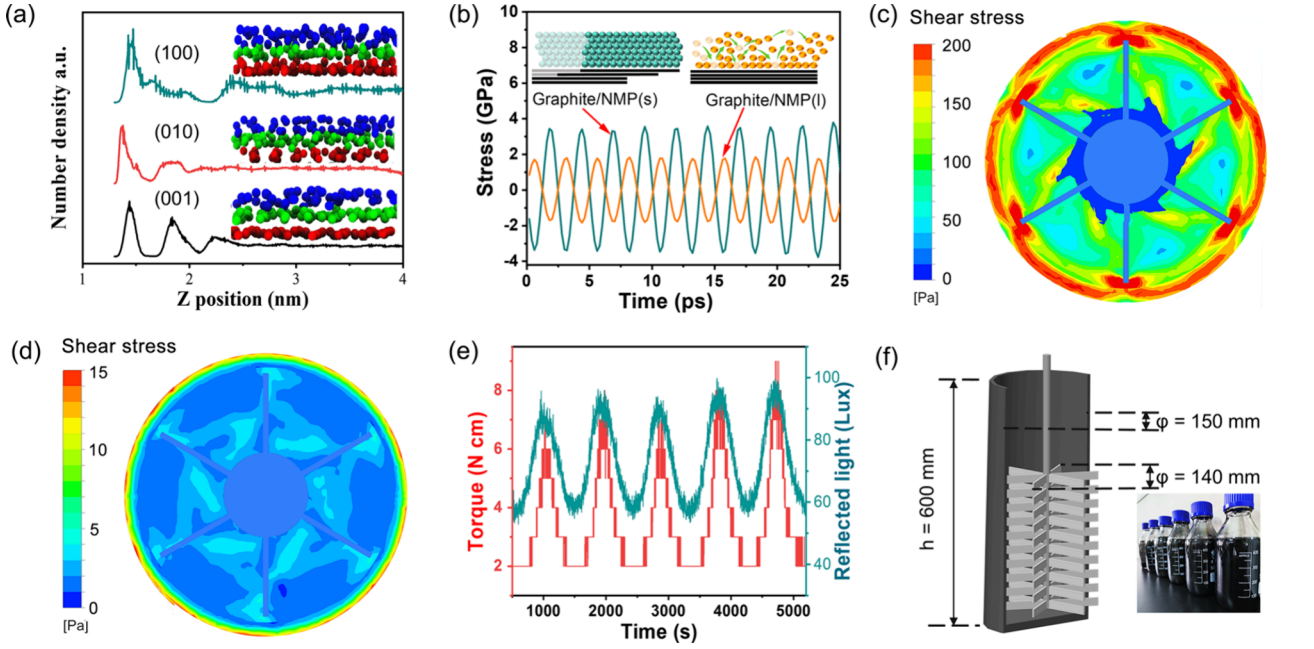

Figure 3. (a) Radial distribution function of NMP molecules on three planes of graphite obtained by MD simulations. The inset shows the distribution of NMP molecules. (b) Shear stress on the graphite/NMP(l) interface and the graphite/NMP(s) interface obtained by MD simulations. Comparison of shear stress distribution for (c) PFS and (d) liquid-based suspension. (e) Reflected light intensity of the suspension and the corresponding torque curve. (f) Structure of scale-up tank and optical photograph of graphene dispersions obtained from a single-shot exfoliation using the tank.

needed in a high-shear mixer, kitchen mixer, or high-pressure homogenizer as previously reported for graphite exfoliation. The energy consumption in PFE, calculated by the torque of the stirrer and the yield of graphene (Supplementary Section 2) is 3.49×10^4 J g^{-1} in PFS, much lower than those in traditional LPE, which typically exceeds 10^6 J g^{-1}, as shown in Figure 1e. That is, the utilization rate of input mechanical energy has been enhanced by 10^2~10^3 times compared to LPE.

https://doi.org/10.1021/acs.nanolett.4c04329
Nano Lett. 2024, 24, 14102−14108

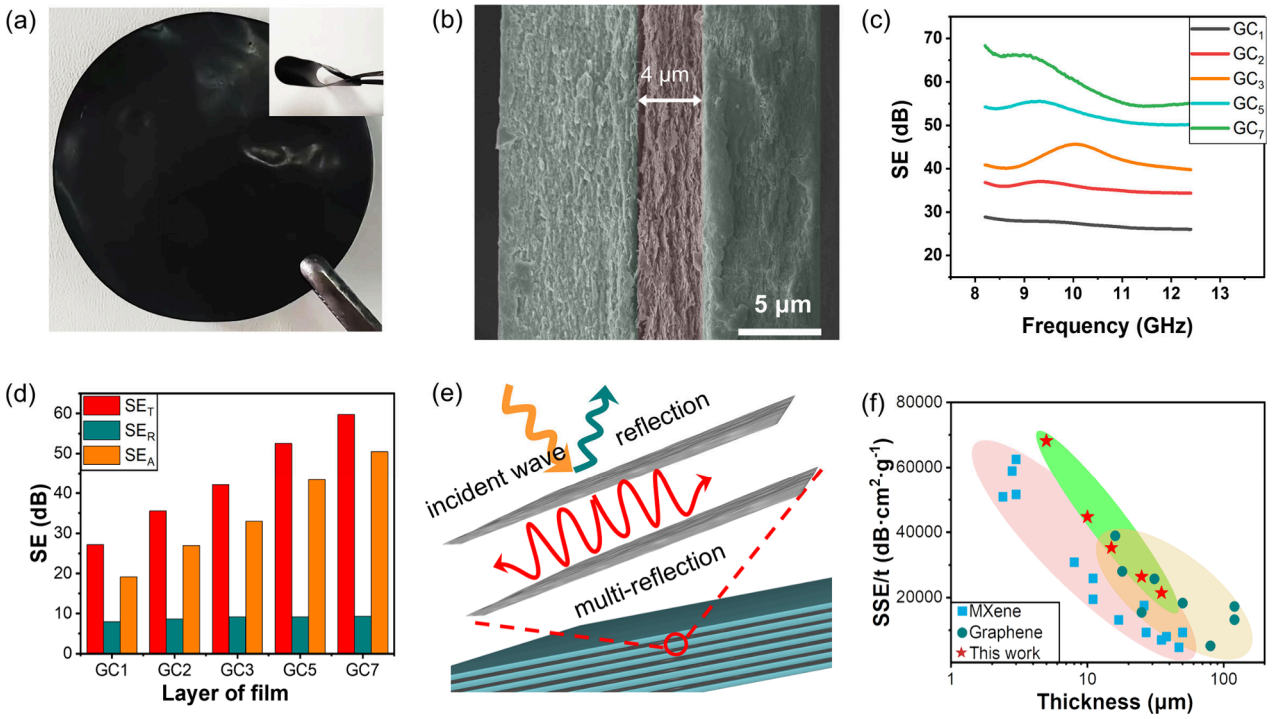

Figure 4. (a) Optical photograph of a cellulose/graphene/cellulose film with inset showing the flexibility. (b) The cross-section of the cellulose/graphene/cellulose film. (c) EMI shielding effectiveness of films with different numbers of layers, where GC_x indicates that x layers of sandwich films are stacked. (d) Proportion of reflection and absorption in the shielding effectiveness. (e) Electromagnetic wave shielding mechanism diagram of multilayer composite shielding film. (f) Specific shielding effectiveness of cellulose/graphene/cellulose films compared to the previously reported values (Supplementary Section 12).

Figure 2a shows the graphene dispersion obtained by diluting the supernatant of centrifugation at 2000 rpm to 0.015 g L^{-1}, from which the Tyndall effect is clearly observed, indicating a colloidal state of the exfoliated graphite in NMP (the dispersion ability of graphene in various solvents is presented in Supplementary Section 3). The typical AFM image of the suspension in Figure 2b shows that there are two representative graphene flakes in the dispersion: one is in a strip shape with a width of 400−600 nm and a length of 1.5−2.5 μm, and the other one has an irregular shape with a lateral size of 300−600 nm, as statistically illustrated in Figure 2c. The thickness distribution for the strip flakes peaks at around 4 nm and that for small flakes at about 1.4 nm, as shown in Figure 2d. To find out the reason why two distinct flakes are obtained, a high-speed camera was used to observe the crystal morphology of NMP in the stirring, and the optical image is shown in Figure S5f. It is found that the frozen NMP crystal shows a rod-like morphology, which may be related to the production of strip shape flakes as the frozen NMP has a stronger interaction with graphite during the exfoliation. Two kinds of flakes can be further separated by fractional centrifugation: a centrifugal speed of 2000−2500 rpm mainly results in the strip flakes, and for a centrifugal speed more than 6000 rpm, small flakes remain in the supernatant (Supplementary Section 4).

The XPS spectra (Supplementary Section 5) show that they are free of impurities other than oxygen in the graphene flakes obtained. The strip flakes have a C:O ratio of 36:1, and the small flakes have a C:O of 22:1. As illustrated in the C 1s curves in Figure 2e, two oxygenic groups (C−O, 286 eV; C=O, 287.5 eV) are identified from both types of flakes.[40] The fraction of sp^3 carbon obtained from XPS is enhanced from 25.7% for strip flakes to 31.6% for small flakes. The Raman spectra shown in Figure 2f show a ratio of the D peak to G peak (I_D/I_G) of 0.29 for strip flakes and 1.26 for small flakes, both higher than 0.08 for raw graphite before exfoliation. Compared to strip flakes, the small flakes exhibit enhanced levels of oxygen content, sp^3 carbon atoms, and the I_D/I_G ratio. This improvement can be attributed to the presence of a higher number of edge atoms or topological defects induced during exfoliation.

To understand the mechanism behind the largely improved energy utilization efficiency of PFE, the microscopic interface between frozen NMP and graphite was investigated with molecular dynamics (MD) simulations (Supplementary Section 6). First, the radial distribution function and diffusivity of NMP molecules are compared for each crystal plane of graphite, as shown in Figure 3a. Along the direction perpendicular to the (001) plane of graphite (i.e., c axis of stacking), three distribution peaks can be identified in the distance of interest, while only a single prominent distribution peak is observed on the other two planes, indicating the higher ordering of NMP molecules on the graphite (001) plane. Concurrently, the diffusion coefficient of NMP on the (001) plane is calculated as 2.1×10^{-12} m^2 s^{-1}, much lower than 3.5×10^{-11} m^2 s^{-1} on the (010) plane and 2.6×10^{-11} m^2 s^{-1} on the (100) plane, showing that the NMP molecules are more immobile due to the stronger adsorption on the (001) plane of graphite.

Upon lowering the temperature to the freezing point of NMP, the adhesion between solid NMP (NMP(s)) and graphite is further enhanced. To verify the interfacial stress transfer brought by freezing, two sandwich structures in which graphite is wrapped with liquid or solid NMP were

https://doi.org/10.1021/acs.nanolett.4c04329
Nano Lett. 2024, 24, 14102−14108

constructed, and the interfacial stress was simulated with MD. As shown in Figure 3b, the maximal stress reaches 3.5 GPa in the NMP(s) model, higher than 1.6 GPa simulated from the liquid NMP (NMP(l)) model. The periodic fluctuation with time generated in MD corresponds to the dynamic establishment of optimal adsorption in the constant deformation model. Figures S8a and S8b shows that the slipping of NMP at the NMP(s)/graphite interface is suppressed, and the slipping of graphene layers in graphite is enhanced. By using a pair of graphite in contact with NMP, the tensile limit of the loading was tested (Supplementary Section 6), from which we can estimate that the shear strength of the interface has been improved from 40 N m^{-2} for the NMP(l)/graphite interface to 10^5 N m^{-2} for the NMP(s)/graphite interface. Such an enhancement of interfacial shear strength ensures that the shear force in the flow can be efficiently transferred to the graphite, rather than being lost at the interface.

Now we discuss the effect of flow on the shear force. In PFS, the presence of NMP crystals changes the fluid from a turbulent to a laminar feature. The rheology properties of the suspension are measured (Supplementary Section 8), and the shear stress distribution of the suspension (Supplementary Section 9) is explored. As shown in Figure 3c, the shear stress for PFS in the tank is above 100 Pa and can be as high as 200 Pa at the end of the stirring blade, much higher than the typical shear stress of less than 2 Pa before cooling (Figure 3d). The two orders of enhancement in shear stress of the flow would further improve the conversion of the input mechanical energy to energy applicable in graphite exfoliation. Figure 3e shows that the reflection intensity by graphite (method described in Supplementary Section 10) periodically fluctuates with the torque change, which was measured in a glovebox to minimize the interference of water vapor, indicating that the graphite particles have been oriented along the direction of flow in PFS. Thus, the shear force would apply more on the graphite exfoliation rather than on breaking graphite.

The current strategy is ready for scale up. Based on the understanding of the shear stress distribution in PFS, a 10 L stir tank is designed for high shear and low turbulence conditions, as illustrated in Figure 3f, based on which a shear stress of 200 Pa near the tank wall was confirmed by CFD simulation. After processing 6 L of suspension of 600 g of graphite for 3 h, a graphene concentration of 2.56 gL^{-1} is achieved, comparable to 2.32 g L^{-1} obtained in a 0.4 L beaker prepared under the same conditions. The results indicate that the laminar feature inside the PFS ensures a stable and controllable high-shear environment, which gives the PFE a great potential for scale up by reducing the scaling effect due to the minimized dead zone by the more uniform fluidic gradient in PFE.[41] The PFE strategy was also employed to exfoliate other layered materials, such as hexagonal boron nitride and mica, demonstrating the versatility of the method (Supplementary Section 11).

For state-of-the-art EMI shielding, the excellent electrical conductivity of the constituent material is a prerequisite.[28,42−44] Figure 4a shows a cellulose/graphene/cellulose sandwich film that is flexible and has a clear interface between graphene and cellulose. Wrapped by a cellulose layer with a thickness of 8 μm, the inner 4 μm thick graphene layer has an electrical conductivity of 2×10^4 S m^{-1}, as shown in Figure 4b. The EMI shielding in Figure 4c shows that a single sandwich film achieves shielding effectiveness of ∼27 dB, while ∼60 dB is achieved from seven layers. The film produces the higher absorption in the low frequency band in the range of interest, which is consistent with the reported performance of carbon-based materials showing an SE curve fluctuating with frequency.[45−47]

Detailed in Figure 4d, the results indicate that when the surface reflects 90% of the electromagnetic wave, the graphene layer absorbs most of the residual electromagnetic wave. The multilayer structure offers multiple interfaces for electromagnetic wave reflection, which promotes multiple reflection and absorption of electromagnetic waves between the multigraphene layers, as schematically shown in Figure 4e. Due to the low density of graphene films (0.98 g cm^{-3}), the composite film demonstrates superior specific shielding efficiency (SSE/t) up to 6.8×10^4 dB cm^2 g^{-1}. This value is better than most reported graphene-based materials[22,27,48] and superior to MXene at equivalent thicknesses,[49−52] as compared in Figure 4f (the details are in Supplementary Section 11). The outstanding electromagnetic shielding capability of such films justifies the demand of light and flexible structures for the rapid advancement of miniaturized electronic devices and wireless communication.[53,54]

In summary, we have developed a PFE strategy to prepare graphene platelets in partially freezing NMP, showing a high production efficiency (0.78 g L^{-1} h^{-1}) achieved at the ultralow shear rate (350 s^{-1}). In this way, the mechanical energy consumption has been lowered to 3.49×10^4 J g^{-1}, showing an efficiency enhancement of 10^2∼10^3 times that in conventional LPE. Simulations show that the freezing of NMP has greatly enhanced the internal shear stress of PFS and thus the transfer of shear force to the graphite (001) surface by aligning the orientation of graphite along the flow direction in a laminar flow. When being assembled into stacking films, the graphene provides a specific shielding efficiency (SSE/t) reaching 6.8×10^4 dB cm^{-1} g^{-1}. This work presents an efficient, low-energy, yet sustainable strategy for producing high-quality graphene, potentially useful for other two-dimensional nanomaterials at the industrial scale.

■ ASSOCIATED CONTENT

Supporting Information

The Supporting Information is available free of charge at https://pubs.acs.org/doi/10.1021/acs.nanolett.4c04329.

Detailed process of graphene preparation by PFE and fabrication of graphene films; the flow state of the suspension; the SEM, TEM morphology, and XPS of the graphene obtained by PFE, the changes in the flow field at the interface and suspension when NMP is frozen; the orientation measurement of graphite; and data on electromagnetic shielding films mentioned in Figure 4f (PDF)

Movie S1, the flow state of the suspension before NMP is partially frozen (MP4)

Movie S2, the flow state of the suspension after NMP is partially frozen (MP4)

■ AUTHOR INFORMATION

Corresponding Authors

Jingwei Zhang − *National and Local Joint Engineering Research Center for Applied Technology of Hybrid Nanomaterials, Henan University, Kaifeng 475004, P. R. China;* orcid.org/0000-0002-2261-7605; Email: jwzhang@henu.edu.cn

https://doi.org/10.1021/acs.nanolett.4c04329
Nano Lett. 2024, 24, 14102−14108

Yanwu Zhu − *Hefei National Research Center for Physical Sciences at the Microscale, & School of Chemistry and Materials Science, University of Science and Technology of China, Hefei 230026, P. R. China;* orcid.org/0000-0002-7505-1502; Email: zhuyanwu@ustc.edu.cn

Authors

Kaixiang Pang − *National and Local Joint Engineering Research Center for Applied Technology of Hybrid Nanomaterials, Henan University, Kaifeng 475004, P. R. China;* orcid.org/0009-0005-1866-9348

Xiaoke Fang − *National and Local Joint Engineering Research Center for Applied Technology of Hybrid Nanomaterials, Henan University, Kaifeng 475004, P. R. China*

Chuanren Ye − *Hefei National Research Center for Physical Sciences at the Microscale, & School of Chemistry and Materials Science, University of Science and Technology of China, Hefei 230026, P. R. China;* orcid.org/0000-0003-3346-8948

Yuanhui Wang − *National and Local Joint Engineering Research Center for Applied Technology of Hybrid Nanomaterials, Henan University, Kaifeng 475004, P. R. China*

Linlin Zhao − *National and Local Joint Engineering Research Center for Applied Technology of Hybrid Nanomaterials, Henan University, Kaifeng 475004, P. R. China*

Chunhong Gong − *National and Local Joint Engineering Research Center for Applied Technology of Hybrid Nanomaterials, Henan University, Kaifeng 475004, P. R. China*

Shuaishuai Zhou − *National and Local Joint Engineering Research Center for Applied Technology of Hybrid Nanomaterials, Henan University, Kaifeng 475004, P. R. China*

Gai Zhao − *State Key Laboratory of Mechanics and Control for Aerospace Structures, Nanjing University of Aeronautics and Astronautics, Nanjing 210016, P. R. China;* orcid.org/0000-0002-6466-4223

Complete contact information is available at: https://pubs.acs.org/10.1021/acs.nanolett.4c04329

Author Contributions

[#]These authors contributed equally (K.P. and X.F.).

Notes

The authors declare no competing financial interest.

■ ACKNOWLEDGMENTS

This work is financially supported by the National Natural Science Foundation of China (Grants U2004176, U2004210, 22475065 and 52325202).

■ REFERENCES

(1) Morozov, S. V.; Novoselov, K. S.; Katsnelson, M. I.; Schedin, F.; Elias, D. C.; Jaszczak, J. A.; Geim, A. K. Giant intrinsic carrier mobilities in graphene and its bilayer. *Phys. Rev. Lett.* **2008**, *100* (1), 016602.

(2) Lee, C.; Wei, X. D.; Kysar, J. W.; Hone, J. Measurement of the elastic properties and intrinsic strength of monolayer graphene. *Science* **2008**, *321* (5887), 385−388.

(3) Yu, C. H.; Shi, L.; Yao, Z.; Li, D. Y.; Majumdar, A. Thermal conductance and thermopower of an individual single-wall carbon nanotube. *Nano Lett.* **2005**, *5* (9), 1842−1846.

(4) Ghosh, S.; Bao, W.; Nika, D. L.; Subrina, S.; Pokatilov, E. P.; Lau, C. N.; Balandin, A. A. Dimensional crossover of thermal transport in few-layer graphene. *Nat. Mater.* **2010**, *9* (7), 555−8.

(5) Novoselov, K. S.; Geim, A. K.; Morozov, S. V.; Jiang, D.; Zhang, Y.; Dubonos, S. V.; Grigorieva, I. V.; Firsov, A. A. Electric field effect in atomically thin carbon films. *Science* **2004**, *306* (5696), 666−669.

(6) Balandin, A. A. Thermal properties of graphene and nanostructured carbon materials. *Nat. Mater.* **2011**, *10* (8), 569−581.

(7) Dai, W.; Lv, L.; Ma, T.; Wang, X.; Ying, J.; Yan, Q.; Tan, X.; Gao, J.; Xue, C.; Yu, J.; Yao, Y.; Wei, Q.; Sun, R.; Wang, Y.; Liu, T. H.; Chen, T.; Xiang, R.; Jiang, N.; Xue, Q.; Wong, C. P.; Maruyama, S.; Lin, C. T. Multiscale Structural Modulation of Anisotropic Graphene Framework for Polymer Composites Achieving Highly Efficient Thermal Energy Management. *Advanced Science* **2021**, *8* (7), 2003734.

(8) Guo, H. C.; Zhao, H. Y.; Niu, H. Y.; Ren, Y. J.; Fang, H. M.; Fang, X. X.; Lv, R. C.; Maqbool, M.; Bai, S. L. Highly Thermally Conductive 3D Printed Graphene Filled Polymer Composites for Scalable Thermal Management Applications. *ACS Nano* **2021**, *15* (4), 6917−6928.

(9) Yan, Q. W.; Alam, F. E.; Gao, J. Y.; Dai, W.; Tan, X.; Lv, L.; Wang, J. J.; Zhang, H.; Chen, D.; Nishimura, K.; Wang, L. P.; Yu, J. H.; Lu, J. B.; Sun, R.; Xiang, R.; Maruyama, S.; Zhang, H.; Wu, S. D.; Jiang, N.; Lin, C. T. Soft and Self-Adhesive Thermal Interface Materials Based on Vertically Aligned, Covalently Bonded Graphene Nanowalls for Efficient Microelectronic Cooling. *Adv. Funct. Mater.* **2021**, *31* (36), 31.

(10) Xin, G. Q.; Sun, H. T.; Hu, T.; Fard, H. R.; Sun, X.; Koratkar, N.; Borca-Tasciuc, T.; Lian, J. Large-Area Freestanding Graphene Paper for Superior Thermal Management. *Adv. Mater.* **2014**, *26* (26), 4521−4526.

(11) Raccichini, R.; Varzi, A.; Passerini, S.; Scrosati, B. The role of graphene for electrochemical energy storage. *Nat. Mater.* **2015**, *14* (3), 271−279.

(12) Li, Z.; Gadipelli, S.; Li, H.; Howard, C. A.; Brett, D. J. L.; Shearing, P. R.; Guo, Z.; Parkin, I. P.; Li, F. Tuning the interlayer spacing of graphene laminate films for efficient pore utilization towards compact capacitive energy storage. *Nature Energy* **2020**, *5* (2), 160−168.

(13) Gholami Laelabadi, K.; Moradian, R.; Manouchehri, I. One-Step Fabrication of Flexible, Cost/Time Effective, and High Energy Storage Reduced Graphene Oxide@PANI Supercapacitor. *ACS Applied Energy Materials* **2020**, *3* (6), 5301−5312.

(14) Zhou, M.; Guo, S. J. Electrocatalytic Interface Based on Novel Carbon Nanomaterials for Advanced Electrochemical Sensors. *ChemCatChem.* **2015**, *7* (18), 2744−2764.

(15) Antiochia, R.; Gorton, L. A new osmium-polymer modified screen-printed graphene electrode for fructose detection. *Sensor Actuat B-Chem.* **2014**, *195*, 287−293.

(16) Kim, J. E.; Han, T. H.; Lee, S. H.; Kim, J. Y.; Ahn, C. W.; Yun, J. M.; Kim, S. O. Graphene Oxide Liquid Crystals. *Angew. Chem., Int. Ed.* **2011**, *50* (13), 3043−3047.

(17) Hernandez, Y.; Nicolosi, V.; Lotya, M.; Blighe, F. M.; Sun, Z. Y.; De, S.; McGovern, I. T.; Holland, B.; Byrne, M.; Gun'ko, Y. K.; Boland, J. J.; Niraj, P.; Duesberg, G.; Krishnamurthy, S.; Goodhue, R.; Hutchison, J.; Scardaci, V.; Ferrari, A. C.; Coleman, J. N. High-yield production of graphene by liquid-phase exfoliation of graphite. *Nat. Nanotechnol.* **2008**, *3* (9), 563−568.

(18) Arao, Y.; Mizuno, Y.; Araki, K.; Kubouchi, M. Mass production of high-aspect-ratio few-layer-graphene by high-speed laminar flow. *Carbon* **2016**, *102*, 330−338.

(19) Paton, K. R.; Varrla, E.; Backes, C.; Smith, R. J.; Khan, U.; O'Neill, A.; Boland, C.; Lotya, M.; Istrate, O. M.; King, P.; Higgins, T.; Barwich, S.; May, P.; Puczkarski, P.; Ahmed, I.; Moebius, M.; Pettersson, H.; Long, E.; Coelho, J.; O'Brien, S. E.; McGuire, E. K.; Sanchez, B. M.; Duesberg, G. S.; McEvoy, N.; Pennycook, T. J.; Downing, C.; Crossley, A.; Nicolosi, V.; Coleman, J. N. Scalable production of large quantities of defect-free few-layer graphene by shear exfoliation in liquids. *Nat. Mater.* **2014**, *13* (6), 624−630.

(20) Chen, X.; Dobson, J. F.; Raston, C. L. Vortex fluidic exfoliation of graphite and boron nitride. *Chem. Commun.* **2012**, *48* (31), 3703.
(21) Narayan, R.; Kim, S. O. Surfactant mediated liquid phase exfoliation of graphene. *Nano Convergence* **2015**, *2* (1), 20.
(22) Liu, X.; Chen, T.; Liang, H.; Qin, F.; Yang, H.; Guo, X. Facile approach for a robust graphene/silver nanowires aerogel with high-performance electromagnetic interference shielding. *RSC Adv.* **2019**, *9* (1), 27−33.
(23) Wang, Y. C.; Yao, L. H.; Zheng, Q.; Cao, M. S. Graphene-wrapped multiloculated nickel ferrite: A highly efficient electromagnetic attenuation material for microwave absorbing and green shielding. *Nano Research* **2022**, *15* (7), 6751−6760.
(24) Lai, D. G.; Chen, X. X.; Wang, Y. Controllable fabrication of elastomeric and porous graphene films with superior foldable behavior and excellent electromagnetic interference shielding performance. *Carbon* **2020**, *158*, 728−737.
(25) Xu, F.; Chen, R. F.; Lin, Z. S.; Sun, X. X.; Wang, S. S.; Yin, W. L.; Peng, Q. Y.; Li, Y. B.; He, X. D. Variable densification of reduced graphene oxide foam into multifunctional high-performance graphene paper. *Journal Of Materials Chemistry C* **2018**, *6* (45), 12321−12328.
(26) Paliotta, L.; De Bellis, G.; Tamburrano, A.; Marra, F.; Rinaldi, A.; Balijepalli, S. K.; Kaciulis, S.; Sarto, M. S. Highly conductive multilayer-graphene paper as a flexible lightweight electromagnetic shield. *Carbon* **2015**, *89*, 260−271.
(27) Liang, J.; Wang, Y.; Huang, Y.; Ma, Y.; Liu, Z.; Cai, J.; Zhang, C.; Gao, H.; Chen, Y. Electromagnetic interference shielding of graphene/epoxy composites. *Carbon* **2009**, *47* (3), 922−925.
(28) Chen, Y.; Wang, Y.; Zhang, H.-B.; Li, X.; Gui, C.-X.; Yu, Z.-Z. Enhanced electromagnetic interference shielding efficiency of polystyrene/graphene composites with magnetic Fe3O4 nanoparticles. *Carbon* **2015**, *82*, 67−76.
(29) Tao, H.; Zhang, Y.; Gao, Y.; Sun, Z.; Yan, C.; Texter, J. Scalable exfoliation and dispersion of two-dimensional materials - an update. *Phys. Chem. Chem. Phys.* **2017**, *19* (2), 921−960.
(30) Khan, U.; O'Neill, A.; Lotya, M.; De, S.; Coleman, J. N. High-Concentration Solvent Exfoliation of Graphene. *Small* **2010**, *6* (7), 864−871.
(31) Wang, W.; Dai, S. Y.; Li, X. D.; Yang, J. R.; Srolovitz, D. J.; Zheng, Q. S. Measurement of the cleavage energy of graphite. *Nat. Commun.* **2015**, *6*, 7853.
(32) Zacharia, R.; Ulbricht, H.; Hertel, T. Interlayer cohesive energy of graphite from thermal desorption of polyaromatic hydrocarbons. *Phys. Rev. B* **2004**, *69* (15), 155406.
(33) Roenbeck, M. R.; Wei, X. D.; Beese, A. M.; Naraghi, M.; Furmanchuk, A.; Paci, J. T.; Schatz, G. C.; Espinosa, H. D. Scanning Electron Microscope Peeling To Quantify Surface Energy between Multiwalled Carbon Nanotubes and Graphene. *ACS Nano* **2014**, *8* (1), 124−138.
(34) Bourlinos, A. B.; Georgakilas, V.; Zboril, R.; Steriotis, T. A.; Stubos, A. K. Liquid-Phase Exfoliation of Graphite Towards Solubilized Graphenes. *Small* **2009**, *5* (16), 1841−1845.
(35) Thi, Q. H.; Man, P.; Liu, H.; Huang, L.; Chen, X.; Lee, C.-S.; Zhao, J.; Deng, Q.; Saeed, S.; Ly, T. H. Ultrahigh Lubricity between Two-Dimensional Ice and Two-Dimensional Atomic Layers. *Nano Lett.* **2023**, *23* (4), 1379−1385.
(36) Fang, X.; Pang, K.; Zhao, G.; Wang, Y.; Zhang, W.; Zhang, Y.; Zhou, S.; Zhang, J.; Gong, C. Improving the liquid phase exfoliation efficiency of graphene based on the enhanced intermolecular and interfacial interactions. *Chemical Engineering Journal* **2024**, *480*, 148263.
(37) Uysal Unalan, I.; Wan, C.; Trabattoni, S.; Piergiovanni, L.; Farris, S. Polysaccharide-assisted rapid exfoliation of graphite platelets into high quality water-dispersible graphene sheets. *RSC Adv.* **2015**, *5* (34), 26482−26490.
(38) Zhao, W.; Fang, M.; Wu, F.; Wu, H.; Wang, L.; Chen, G. Preparation of graphene by exfoliation of graphite using wet ball milling. *J. Mater. Chem.* **2010**, *20* (28), 5817−5819.
(39) Varrla, E.; Paton, K. R.; Backes, C.; Harvey, A.; Smith, R. J.; McCauley, J.; Coleman, J. N. Turbulence-assisted shear exfoliation of graphene using household detergent and a kitchen blender. *Nanoscale* **2014**, *6* (20), 11810−11819.
(40) Liu, L.; Shen, Z.; Zhang, X.; Ma, S. Low-temperature treatment for preservation and separation of graphene dispersions. *J. Mater. Sci.* **2018**, *53* (19), 13875−13885.
(41) Kelly, W.; Gigas, B. Using CFD to predict the behavior of power law fluids near axial-flow impellers operating in the transitional flow regime. *Chem. Eng. Sci.* **2003**, *58* (10), 2141−2152.
(42) Fang, X.; Zhang, Y.; Pang, K.; Wang, Y.; Hu, T.; Zhang, W.; Gong, C.; Zhang, J. In situ construction of efficient electromagnetic function Graphene/PES composites based on liquid phase exfoliation strategy. *Materials Today Physics* **2024**, *43*, 101408.
(43) Zhou, X.; Min, P.; Liu, Y.; Jin, M.; Yu, Z.-Z.; Zhang, H.-B. Insulating electromagnetic-shielding silicone compound enables direct potting electronics. *Science* **2024**, *385* (6714), 1205−1210.
(44) Si, H.; Zhang, Y.; Liu, Y.; Jiang, Z.; Li, C.; Zhang, J.; Huang, X.; Gong, C. Structural design in reduced graphene oxide (RGO) metacomposites for enhanced microwave absorption in wide temperature spectrum. *Journal of Materials Science & Technology* **2025**, *206*, 211−220.
(45) Wan, Y. J.; Zhu, P. L.; Yu, S. H.; Sun, R.; Wong, C. P.; Liao, W. H. Graphene paper for exceptional EMI shielding performance using large-sized graphene oxide sheets and doping strategy. *Carbon* **2017**, *122*, 74−81.
(46) Chen, M. T.; Zhang, L.; Duan, S. S.; Jing, S. L.; Jiang, H.; Luo, M. F.; Li, C. Z. Highly conductive and flexible polymer composites with improved mechanical and electromagnetic interference shielding performances. *Nanoscale* **2014**, *6* (7), 3796−3803.
(47) Gupta, S.; Tai, N. H. Carbon materials and their composites for electromagnetic interference shielding effectiveness in X-band. *Carbon* **2019**, *152*, 159−187.
(48) Cao, W. T.; Chen, F. F.; Zhu, Y. J.; Zhang, Y. G.; Jiang, Y. Y.; Ma, M. G.; Chen, F. Binary Strengthening and Toughening of MXene/Cellulose Nanofiber Composite Paper with Nacre-Inspired Structure and Superior Electromagnetic Interference Shielding Properties. *ACS Nano* **2018**, *12* (5), 4583−4593.
(49) Shahzad, F.; Alhabeb, M.; Hatter, C. B.; Anasori, B.; Man Hong, S.; Koo, C. M.; Gogotsi, Y. Electromagnetic interference shielding with 2D transition metal carbides (MXenes). *Science* **2016**, *353* (6304), 1137−1140.
(50) Lipton, J.; Weng, G. M.; Alhabeb, M.; Maleski, K.; Antonio, F.; Kong, J.; Gogotsi, Y.; Taylor, A. D. Mechanically strong and electrically conductive multilayer MXene nanocomposites. *Nanoscale* **2019**, *11* (42), 20295−20300.
(51) Zhang, J.; Kong, N.; Uzun, S.; Levitt, A.; Seyedin, S.; Lynch, P. A.; Qin, S.; Han, M.; Yang, W.; Liu, J.; Wang, X.; Gogotsi, Y.; Razal, J. M. Scalable Manufacturing of Free-Standing, Strong Ti3C2Tx MXene Films with Outstanding Conductivity. *Adv. Mater.* **2020**, *32* (23), 2001093.
(52) Wan, Y.; Xiong, P.; Liu, J.; Feng, F.; Xun, X.; Gama, F. M.; Zhang, Q.; Yao, F.; Yang, Z.; Luo, H.; Xu, Y. Ultrathin, Strong, and Highly Flexible Ti3C2Tx MXene/Bacterial Cellulose Composite Films for High-Performance Electromagnetic Interference Shielding. *ACS Nano* **2021**, *15* (5), 8439−8449.
(53) Zhuang, Z. T.; Chen, H. W.; Li, C. Robust Pristine MXene Films with Superhigh Electromagnetic Interference Shielding Effectiveness via Spatially Confined Evaporation. *ACS Nano* **2023**, *17* (11), 10628−10636.
(54) Liu, J.; Zhang, H. B.; Sun, R. H.; Liu, Y. F.; Liu, Z. S.; Zhou, A. G.; Yu, Z. Z. Hydrophobic, Flexible, and Lightweight MXene Foams for High-Performance Electromagnetic-Interference Shielding. *Adv. Mater.* **2017**, *29* (38), 1702367.

https://doi.org/10.1021/acs.nanolett.4c04329
Nano Lett. 2024, 24, 14102−14108